VECC/EQG/99-01

Jan. 1999

Performance of a Small Scale Prototype of Cellular Honeycomb Proportional Chamber

M.M. Aggarwal[a], Z. Ahammed[b], P.V.K.S. Baba[c], A.K. Bhati[a], S. Chattopadhyay[b], A.K. Dubey[d], M.R. Dutta Mazumdar[b], D.P. Mahapatra[d], M.S. Ganti[b], T.K. Nayak[b], R.N. Singaraju[b], M.D. Trivedi[b] and Y.P. Viyogi[b]

[a] Panjab University, Chandigarh

[b] Variable Energy Cyclotron Centre, Calcutta

[c] Jammu University, Jammu

[d] Institute of Physics, Bhubaneswar

Abstract

Beam test results for the first small-scale prototype of a honeycomb cellular proportional chamber to be used in ALICE PMD are presented. The overall efficiency for MIP detection is found to be around 93%. The efficiency drops to about 75% at the corners of the hexagon. Improvement in design is suggested.

1 Introduction

A preshower photon multiplicity detector (PMD) has been proposed to be implemented in the ALICE experiment for measuring the multiplicity of photons in the forward region [1]. After detailed simulation of the effects of upstream materials, the pseudorapidity region $1.8 \leq \eta \leq 2.8$ has been found to be the most suitable to place the PMD. The background due to beam pipe increases at larger pseudorapidities and that due to the TPC/ITS structural material increases at smaller pseudorapidities. The basic parameters of the PMD, as deduced from VENUS + GEANT simulations are given in Table I. It will consist of a charged particle veto (CPV) for discriminating charged hadrons and a preshower plane of the sensitive medium behind 3 X_0 thick lead converter. The detector will be placed at 600 cm from the interaction point and will be hung from the magnet door.

It is proposed to have a single technology and same granularity for both the CPV and the PMD for ease of fabrication and maintenance and also for matching the cells directly opposite in the CPV and PMD for efficient discrimination of photons and hadrons [2]. Regarding the technology of the detector our experience with the WA93/WA98 PMDs [3, 4] suggest that the scintillator based detector can be bulky and the readout quite expensive. Silicon based detectors with 1 mm pads are practical [5], but have to be placed closer to the vertex, resulting in large background to the TPC in the ALICE setup, which is not acceptable. Thus our choice gets restricted to gas based detectors, where, fortunately, developments in GASSIPLEX chips [6] has made it possible to conceive a low-cost detector and readout, matching our detector granularity as well as the ALICE experimental conditions.

TABLE I

Basic Parameters of the ALICE PMD System

Patemeters	value
Distance from vertex	600 cm
η-coverage	1.8–2.8
Active area	10 sq.m.
Inner radius	70 cm.
Outer radius	200 cm.
cell size (area)	1 sq.cm.
Number of channels (PMD + CPV)	200K
$< N_\gamma >$ (VENUS, central)	5200

2 Design Considerations

The PMD will handle about 5000 photons and almost similar number of charged particles in one unit of pseudorapidity coverage, particle density per sq.cm. varying between 0.05 and 0.15. Handling such a large particle density in a preshower detector requires special considerations for the detector, in particular, occupancy must be low for efficient discrimination of hadrons from photons.

Based on the experience of WA93/WA98 PMDs and factors like mean photon energy in the η-range under consideration and achievable interaction rate in heavy ion collisions at the LHC (with luminosity figures of 10^{27} and 10^{30} respectively for lead and calcium ions), the following criteria are laid down as important parameters for design :

(a) MIP and photon separation should be good down to lowest possible energy (0.2 GeV),

(b) total noise level in the detector and readout should be $\leq$ 0.1 MIP-equivalent,

(c) it should have large dynamic range, upto about 40 MIPs and possess good linearity over this range,

(d) it should have stable operation at rates extending upto 10^4 particles/sec/cm^2,

(e) the detector material (gas) should be insensitive to neutrons, and

(f) it should be thin so that shower overlap is minimised.

Another important consideration in gas detectors used for calorimetry is the role of low-energy δ-electrons. These electrons are produced at large angles and travel to cells located farther apart. It has been found in early simulation that in large uniform gas volumes, the preshower extends to much larger number of cells than in confined media like scintillators [7]. The solution to this problem is to use isolated gas cells with thin walls. Preliminary simulation studies indicate that a material thickness in the range of 0.2 mm is able to reduce the average number of cells for a preshower by 25% (for 1 GeV photons the average number of cells fired without and with 0.2 mm thick wall being 3.8 and 2.9 respectively for 8 mm gas thickness).

The use of conventional gas detector techniques like the cathode pad chambers having large uniform gas volume and pad readout may be difficult in a high multiplicity environment. Apart from the role of δ-electrons discussed above, pad readout tends to broaden the shower due to induced charges at neighbouring pads. This may lead to large overlap of neighbouring showers. For preshower applications it is desirous that MIPs are confined to essentially one pad. Even

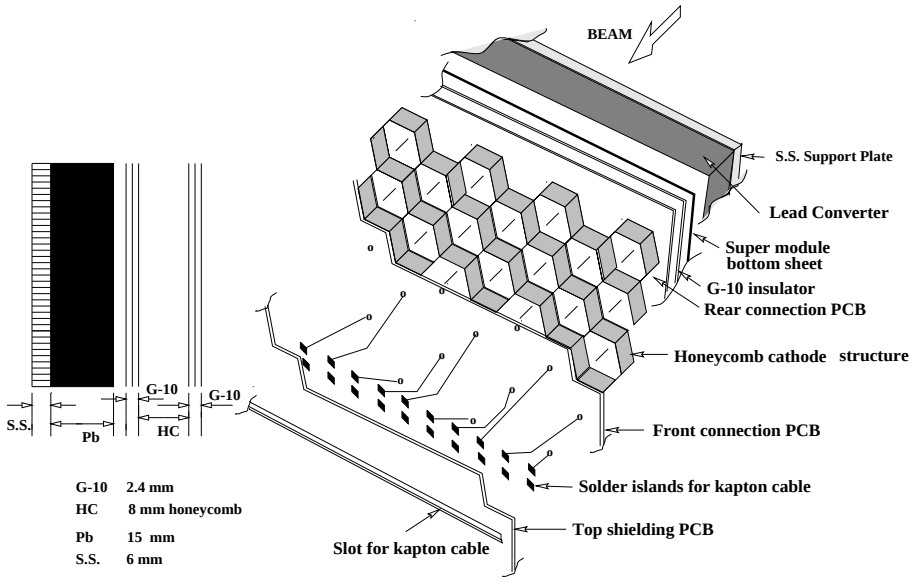

Figure 1: Honeycomb structure for the PMD. A similar structure placed in front of the lead plate acts as the CPV.

for the CPV, more hit pads would mean vetoing of extra photons and hence reducing the photon counting efficiency.

We have therefore selected a design having honeycomb structure and wire readout for the CPV and the PMD as shown in Fig. 1. The basic principle of the detector is similar to that of Ref. [8], but the gas thickness is reduced to our requirements of a preshower detector, and the cells are physically isolated from each other by thin metallic walls. The honeycomb geometry is selected because of its closeness to a circular approximation to provide almost circular equipotentials within a cell. This geometry also facilitates close packing of large arrays.

The honeycomb body forms the common cathode and is kept at large negative potential. The individual anode wires in the cells are kept at ground potential and connected to the readout electronics.

The present design is very different from the conventional proportional chambers and even the design presented in [8] as the ratio of the length of the wire (gas thickness) to the radius of the cell is of the order of unity, which is quite small. The boundary effects in this chamber may be critical and we need to study the performance of the chamber in detail.

3 Prototype Fabrication

A small scale prototype with 96 cells has been fabricated by the following procedure :

Half honeycombs are formed from thin (0.1 mm) copper sheet and joined (spot soldered) to form a row of hex cell structure. Thus, it has 4 sides of 0.1 mm thickness and 2 sides of 0.2 mm thickness, as shown in Fig. 2. It is then coated with graphite paint to improve the aging properties and suppress after-pulsing. Notches are cut at the corners of each half-cell on both lower and upper edges, as shown in Fig. 2 to improve gas conductance within the chamber and to facilitate smooth gas flow within all the cells. A thin teflon coated wire is soldered at one end of the structure, through which a negative high voltage is applied to the cathode. This wire is brought out through a small hole (sealed later) to an SHV connector outside.

The layout of the prototype chamber is schematically shown in Fig. 3. A G-10 frame is machined to house the honeycomb, having 0.5 mm more thickness than the honeycomb to allow tolerances. This frame is fitted on the sides with gas flow nozzles.

Two printed circuit boards (PCBs) of thickness 1.5 mm each are fabricated

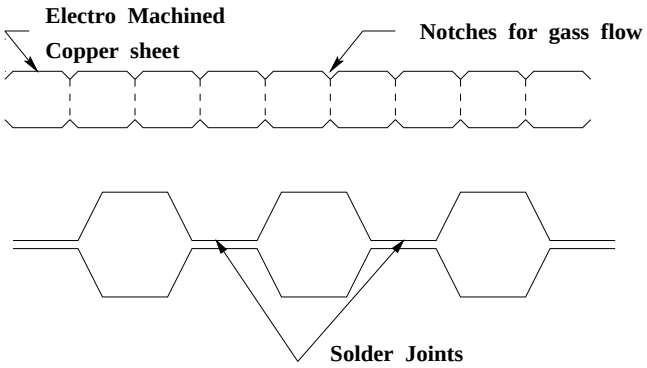

Figure 2: Sketch showing half-row formed from metal pieces

having solder islands (1 mm $\times$ 4 mm) at the center of each cell and thin (0.25 mm) tracks leading to 50 pin ERNI edge connectors as shown in Fig. 4. Only one board has full wiring layout of the tracks, the other having only solder islands to anchor the 20 micron wires. These PCBs have only plain G-10 surface facing the gas side. One PCB is first bonded with epoxy to the G-10 frame. Then the honeycomb is tack-glued to it (edges only) after checking the alignment. The second PCB is then bonded to the other side of the frame after bringing out the cathode (honeycomb) connection.

Gold plated tungsten wires (20 μm dia.) are inserted through the holes of the G10 board using a specially made jig. The jig consists of a small plastic wire spool on an alluminium frame with a hypodermic syringe needle fitted to the frame. The wire is drawn through the capillary of the needle and can be inserted through the PCB holes along with the needle. The needle is withdrawn after tack-soldering the wire onto the rear PCB. The wire can be stretched to a tension of 25-30 gm. using a spring-loaded slider on the spool, before soldering onto the front PCB. Care is taken while soldering to prevent flux creepage on the wire. The holes are then closed by a high viscosity fast setting (5 min.)

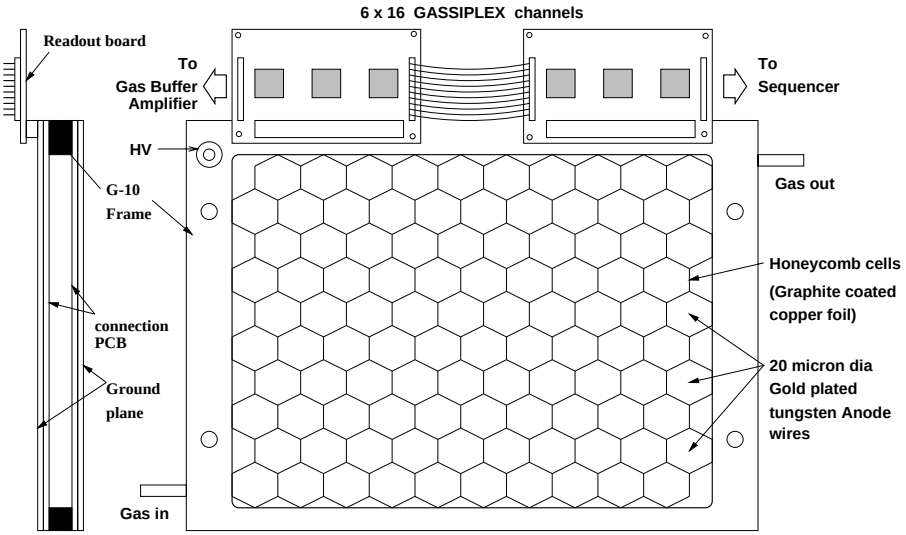

Figure 3: Layout of the hexagonal cells in the prototype chamber. The section at the left shows the G10 frame for the chamber.

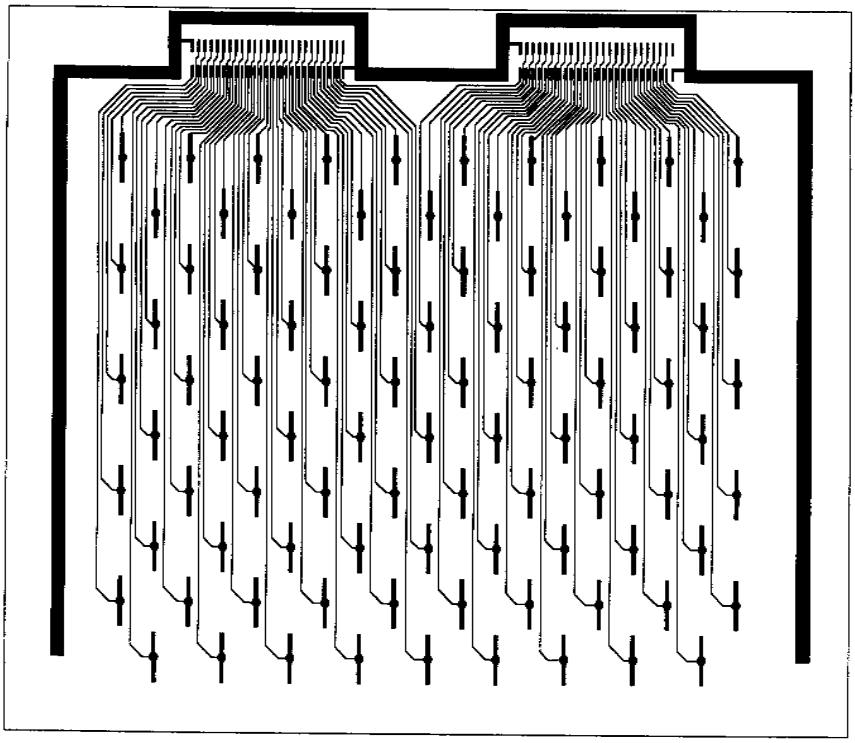

Figure 4: PCB layout for the prototype chamber.

epoxy. Two copper clad printed boards are again bonded on the soldered surface of the above mentioned PCBs, with copper on the outer surface to make a proper shielding for the entire readout connections.

Negative high voltage is fed to the honeycomb cathode through a high value (2.2M) non-inductive resistor with a HV decoupling capacitor.

We tested two prototypes having cell area approx. 130 sq.mm. (radius of the hexagon being 7 mm.). The gas thickness in the chamber was 12 mm and 8 mm in the two cases. The gas used was a mixture of Ar and CO_2.

4 Test Beam Results

4.1 Test Beam Setup

The test setup in the T11 beam-line of the CERN PS is schematically shown in Fig. 5 for tests using pion beam to study the characteristics of the chamber for detecting minimum ionizing particles. It consisted of two sets of microstrip silicon detectors (MSD) for position information on the beam profile. Each MSD had three xy planes covering an area of 1 cm $\times$ 1 cm. Two pairs of scintillators covering an area of 1 cm $\times$ 1 cm. were used for generating triggers, the farthest pair of scintillators being kept behind the prototype chamber. The beam trigger was defined by the four-fold coincidence of the scintillators.

For tests using electron beams to study the preshower characteristics, a lead plate was placed in front of the chamber. In this case the scintillators behind the chamber would not register the beam particles. Hence these were brought in

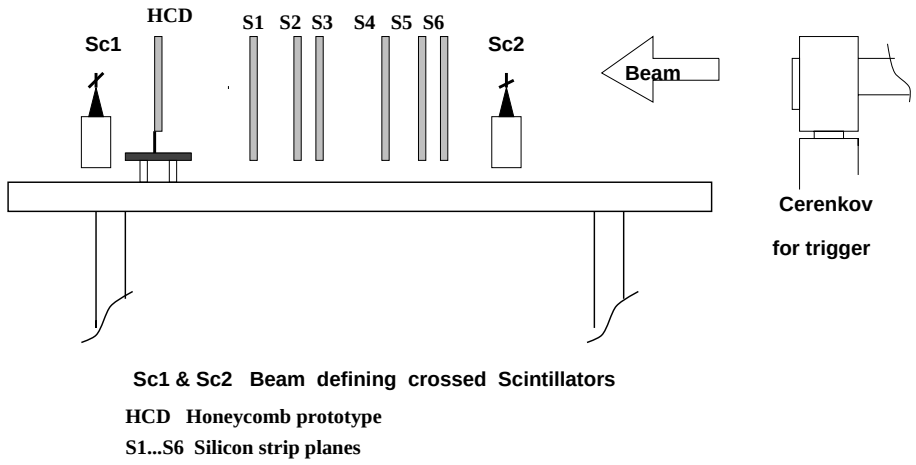

Figure 5: Test setup at the T11 line.

front of the prototype chamber and placed close to it. The MSDs were removed from the beam line as they interposed a lot of material in front of the chamber. A gas cerenkov counter placed upstream was used to discriminate pions and provide the electron trigger.

The pair of scintillators were aligned into the beam line by maximising the individual and coincidence counts. The count rate for the pion beam varied between 20 and 100 per spill of 300 ms duration.

We used gassiplex readout, employing the boards with three chips (48 channels) procured from CERN [9]. The readout chain consisted of the usual devices and the CRAMS based data acquisition system, which also read the MSDs. The pedestals of the gassiplex chips on board the prototype chamber were adjusted to around 60 ADC channels. The RMS of the pedestals was around unity (corresponding to 1200 e^- rms as noise figure) and quite steady throughout the run.

For the present chamber with negative signal from the anode, the dynamic

range of gassiplex is rather low, the output pulse being limited to -1V. With the CRAMS ADC having a range of 1K channels for 1.5 V, we expected a saturation around 700 channels. For the present tests, however, this is not a serious limitation.

4.2 Results for 12 mm Deep Chamber using Pion Beam

The prototype chamber was tested using 3.5 GeV pion beam to study the response to minimum ionising particles (MIP).

4.2.1 Optimisation of Operating Conditions

We studied the efficiency of MIP detection for several combinations of gas mixtures and high voltages. The proportion of Argon in the Ar + CO_2 mixture was kept at 70%, 80% and 90%. The range of HV scanned was 2200 V to 2600 V.

The mip spectra at different values of the HV are shown in Fig. 6. The spectra move to higher channels as the voltage is increased. The saturation near 140 ch. is due to the use of an old buffer card in the gassiplex readout chain. This was subsequently replaced.

The average efficiency is plotted in Fig. 7 as a function of HV. It is found that for the case of Ar : CO_2 at 70:30, the efficiency is almost independent of HV and also close to unity. The optimum value of the gas mixture and the high voltage to be applied to the chamber were selected to be Ar(70%):CO_2(30%) and 2450V.

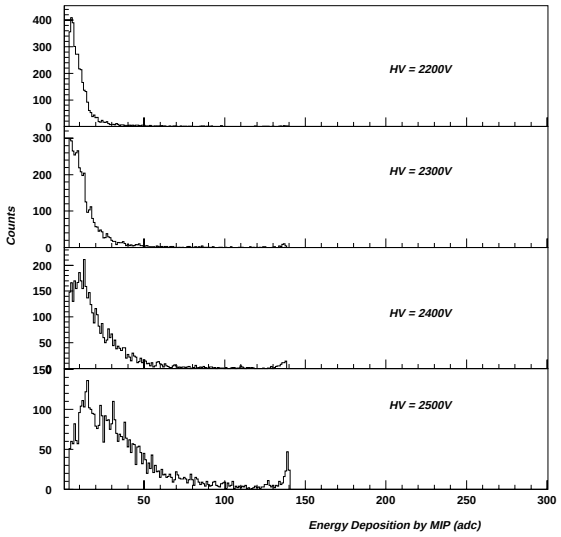

Figure 6: Variation of MIP response with HV for a given gas mixture

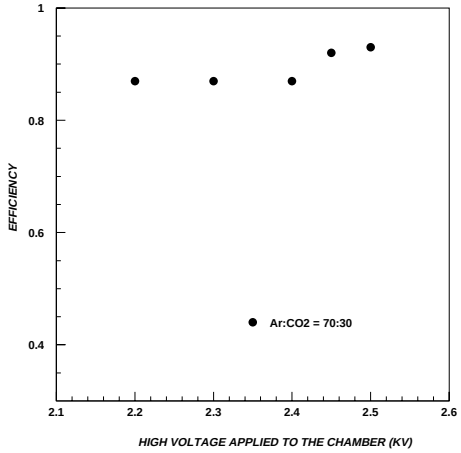

Figure 7: Variation of efficiency of MIP detection with HV for three different gas mixtures.

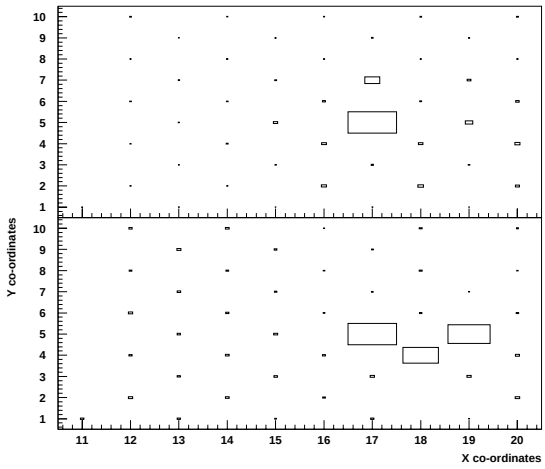

Figure 8: Two-dimensional plot of the cells fired : (a) chamber positioned to allow only one cell to intercept the beam, (b) chamber positioned such that beam hits at the boundary of cells.

4.2.2 Characteristics for MIP Detection

For these studies, the chamber was positioned in such a way that the beam profile was confined to almost one cell. This is shown in the 2-D plot of Fig. 8(a). In some cases we moved the chamber to allow beam to fall near the cell boundaries. The position of the hit cells in such a case is shown in Fig. 8(b).

Fig. 9 shows a typical MIP spectrum and also the number of cells fired by MIPs. It is seen that MIPs are almost confined to within one cell, only about 6% of the MIP cases going to more than one cell. Even when the chamber was positioned such that the beam profile was at the boundary of two cells, the average number of cells fired by MIP did not change substantially.

This result is very significant, suggesting that the cellular design with wire readout is really able to confine the MIP, and that the cross-talk with neigh-

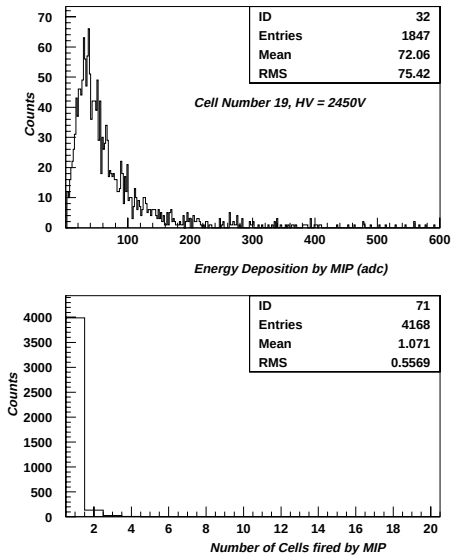

Figure 9: MIP spectrum in a typical cell at 2450 V, and the number of cells fired for MIP

bouring channels is negligible. Considering the fact that the average number of pads fired in WA98 PMD for the MIP case was 3, the present design represents a marked improvement and should allow us to handle the large multiplicity.

When the gas thickness is reduced from 12 mm to 8 mm, the field distribution further worsens. THE shape of the MIP spectrum was found to be not so well defined. The efficiency of MIP detection was aslo quite low, reaching only upto 60%.

4.2.3 Variation of Efficiency within a Cell

The chamber was moved to various positions so as to study the efficiency for various positions within the cell and in particular at the boundaries. The beam profile, as registered in the six planes of the MSDs, is used to study the variation

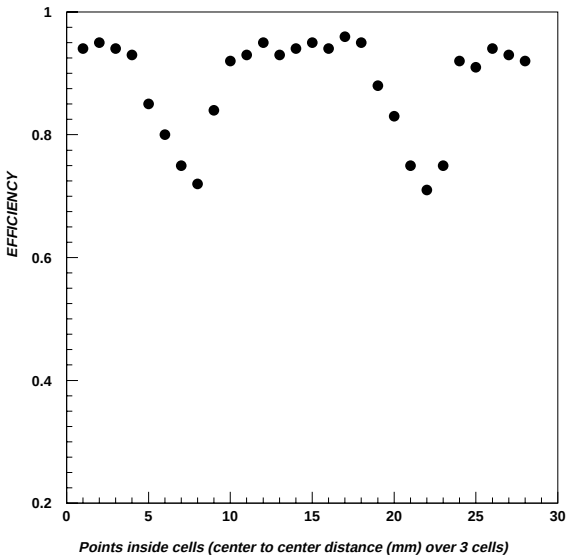

Figure 10: Variation of efficiency of MIP detection as a function of x within a cell.

of efficiency as a function of x- and y- position within a cell.

Fig. 10 shows the variation of efficiency as a function of position in the x-direction covering a full cell and parts of two cells on the sides. It is found that while most part of the cell has almost uniform efficiency around 95%, the efficiency at the boundary is reduced and goes down to about 70% in the extreme edge. This can be easily understood from the hexagonal geometry of the cells, where the field configuration at the edges are distorted.

This result can be understood by considering the simulation results of the field distribution in honeycomb cells using GARFIELD code [10]. Fig. 11 shows the electron drift lines from a primary track entering the cell at 3 mm from the anode wire. It is observed that a substantial fraction of the tracks do not reach

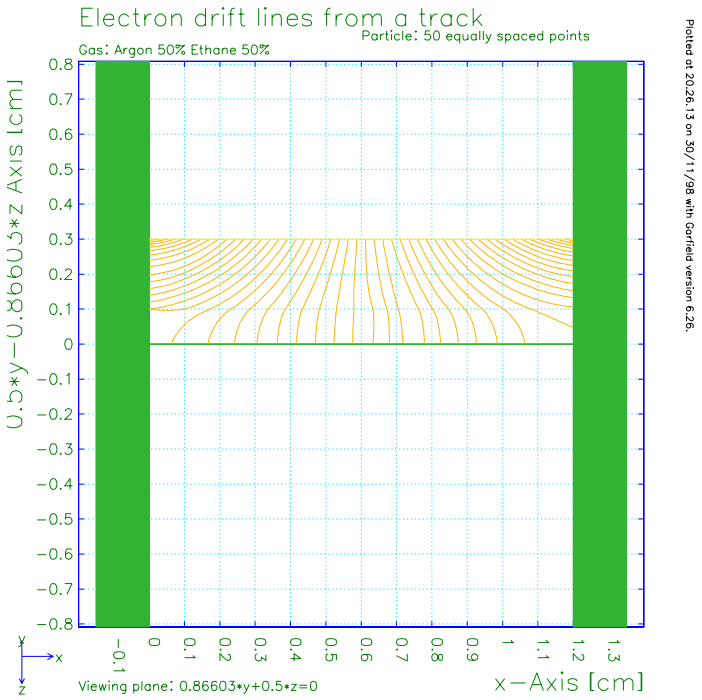

Figure 11: Electron drift lines from garfield simulation for the primary track at 3 mm from the anode. x-axis is along the depth of the chamber, the thick shaded part shows the projection of the G10 plate lids on the plane perpendicular to x-axis.

the anode, instead end up on the G10 plates. The situation is worse for tracks entering the cell farther from the anode. This explains the loss of efficiency at the edges of the cell.

4.2.4 Results for Large Angle Incidence

We have also tested the mip behaviour, in particular the number of pads fired for non-normal incidences. For this purpose the chamber was rotated approximately by 5 deg. and 10 deg. with respect to the beam direction.The average number of cells fired by MIP increases only by a few percent. More precise tests on large

angle incidence will be carried out later.

4.3 Preshower Characteristics using Electron Beam

The T11 beam-line at the PS is not suitable for electron studies, the number of particles are very few and the optics is also not optimum. Using the Cerenkov counter for triggering the electrons, admixture of large fraction of pions cannot be ruled out. Even then we tried to take some data with electron trigger at 3 GeV/c for two different thicknesses of the converter. This may allow us to deduce some information about the preshower behaviour of the chamber.

The preshower spectra, obtained by adding the ADC contents of all the cells in a preshower cluster, are shown in Fig. 12 for the case of 3 GeV/c electrons passing through two different thicknesses of the lead converter as indicated. For this study the gas gain was reduced in order to avoid substantial saturation of the preshower signal in gassiplex. The top part of the above figure shows the corresponding mip spectrum in the central cell where the beam was hitting in the absence of lead converter.

Table II summarises the results on the preshower characteristics of the honeycomb chamber for 3 GeV electrons. It is very encouraging to find that the shower spread is confined to fewer number of pads and are close to the values given by simulation. The somewhat lower value of the average number of cells fired, as compared to that obtained in simulation, is explained by the lower individual cell efficiency. The central cell where the beam hit in the absence of lead converter, had an efficiency of only 70%. Combining this value of the average efficiency and the GEANT results we find that the modified simulation result matches the test data.

TABLE II

Preshower Characteristics for 3 GeV electrons

item	conv. thick. 2 X_0	conv. thick. 3 X_0
Energy Deposition		
data (ADC)	157	223
simulation (keV)	42.6	66.6
ratio	3.7	3.4
no. of cells fired		
data	2.6	3.1
simulation	3.1	4.2

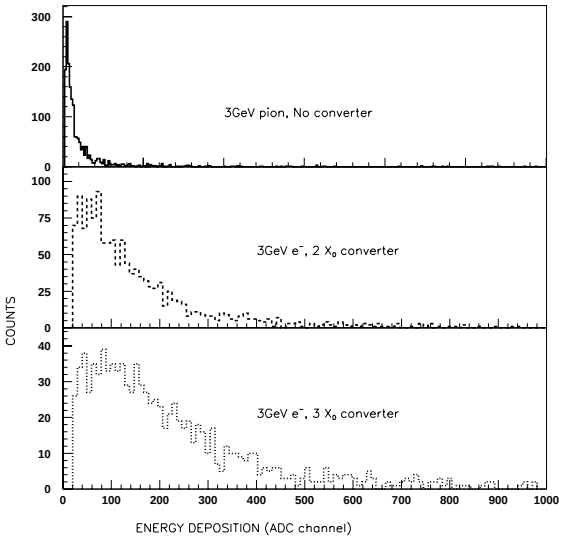

Figure 12: Preshower spectra for 3 GeV electrons with two different thicknesses of the converter

Thus the actual occupancy of the detector will be similar to that given by GEANT simulation results and hence the photon/hadron discrimination algorithm can be applied in a straightforward manner. This is in sharp contrast to

the case of WA93/98 PMDs [3, 4] where the transverse shower spread in test beam data extended to almost twice the number of pads as found in simulation.

A comparison of the values of energy deposition in simulation and test beam data for the two cases of converter thickness also indicate that the chamber behaves almost linearly, although more detailed tests are needed to confirm this behaviour.

4.4 Garfield Simulation and Design Improvements

Use of guard rings has been proposed as one of the techniques for improving the efficiency of the honeycomb chamber near the edges. For this a detailed simulation using GARFIELD code [10] has been undertaken. The hexagonal cell used in this simulation has 6.2 mm side, giving cell area of 1 sq.cm., and 10 mm depth. Preliminary results on the potential distribution for a hexagonal cell without and with two guard rings are shown in Fig. 13 and 14 respectively. The guard rings, each 0.5 mm wide, were placed at 1.7 mm and 3.8 mm from anode. The cathode was kept at -2500 V and the voltage applied to the rings correspond to a logarithmic radial dependence.

A comparison of these two equipotential lines reveals that the use of guard rings greatly helps in orienting the equipotential lines parallel to the anode wire. This will certainly help in increase of primary ionization tracks collecting at the anode and improve the uniformity in the efficiency of the chamber within a cell. Further optimization is in progress by varying the voltages on the rings and the width and location of the rings.

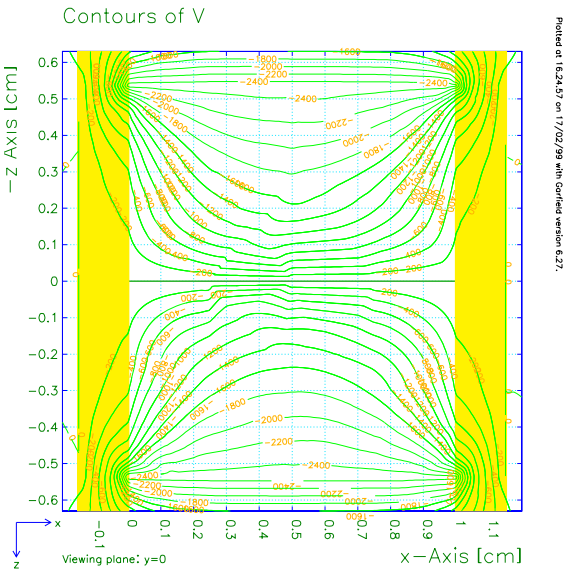

Figure 13: Equipotential lines for a hexagonal cell without guard rings.

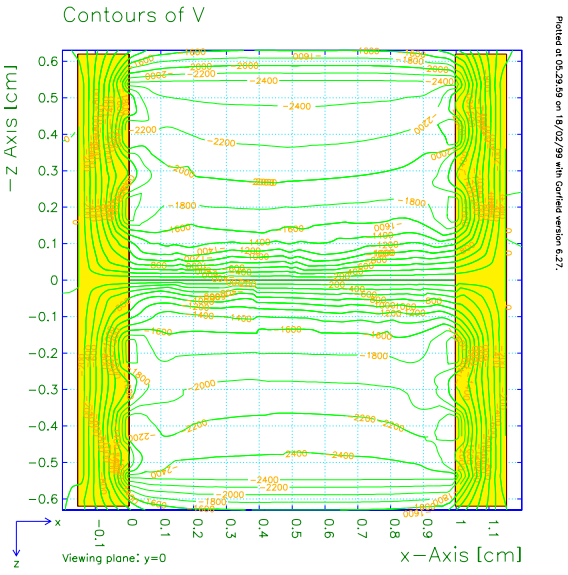

Figure 14: Equipotential lines for a hexagonal cell with guard rings.

5 Future Programme

The present set of results on the behaviour of honeycomb cellular proportional chamber are very encouraging, but several limitations of the design have also been brought out. The most important limitation is the reduction in efficiency at the corners of the honeycomb. For the present geometry of the proportional detector, such a performance is not unexpected.

In actual design of the ALICE PMD, the cell size to be used will be smaller in area than the prototype tested here. This reduction in cell area, which brings the walls closer to the anode wire will help in improving the field distribution. One of the additional suggestions to improve the field uniformity within the cell has been to use the guard-rings [11]. Garfield simulations are in progress to optimise the number of guard rings and the voltages to be applied to them to achieve this goal. A prototype based on the improved design will be tested at the PS during May/June 1999.

Acknowledgements

We acknowledge the help and support provided by F. Piuz, P. Martinengo, T. Williams, A. di Mauro and the PS East Hall staff for the success of these test runs. We thank S. Iranzo for help in using the maxwell code and R. Veenhof for help in running the garfield simulation program.

References

[1] ALICE Technical Proposal, CERN/LHCC 95-71, LHCC/P3, p. 117.

[2] S. Chattopadhyay, Z. Ahammed and Y.P. Viyogi, Nucl. Instr. Meth. sec. A (in press).

[3] M.M. Aggarwal et al, Nucl. Instr. Meth. A372 (1996) 143.

[4] M.M. Aggarwal et al., hep-ex/980726, Nucl. Instr. Meth. sec. A (in press).

[5] Y.P. Viyogi, ALICE Internal Note 98-52 (1998).

[6] J.C. Santiard et al., CERN/ECP/94-17, private communications.

[7] Y.P. Viyogi et al., ALICE Internal Note 95-20 (1995).

[8] V. Balagura, Nucl. Instr. Meth. A368 (1995) 252.

[9] ALICE HMPID TDR, CERN/LHCC 98-19 (1998).

[10] R. Veenhof, CERN Programme Library, entry W5050.

[11] F. Piuz, private communication.